Reconfigurable silicon thermo-optical ring resonator switch based on Vernier effect control

William S. Fegadolli,[1,2,6,*] German Vargas,[4] Xuan Wang,[4] Felipe Valini,[5] Luis A. M. Barea,[5] José E. B. Oliveira,[1] Newton Frateschi,[5] Axel Scherer,[6] Vilson R. Almeida,[1,2] and Roberto R. Panepucci[3,4]

[1] *Instituto Tecnológico de Aeronáutica – ITA, Brazil*
[2] *Instituto de Estudos Avançados – IEAv, Brazil*
[3] *Centro de Tecnologia da Informação Renato Archer – CTI, Brazil*
[4] *Florida International University – FIU, USA*
[5] *Universidade Estadual de Campinas – Unicamp, Brazil*
[6] *California Institute of Technology – Caltech, USA*
[*] *fegadoli@caltech.edu*

Abstract: A proof-of-concept for a new and entirely CMOS compatible thermo-optic reconfigurable switch based on a coupled ring resonator structure is experimentally demonstrated in this paper. Preliminary results show that a single optical device is capable of combining several functionalities, such as tunable filtering, non-blocking switching and reconfigurability, in a single device with compact footprint (~50μm x 30μm).

OCIS codes: (130.3120) Integrated optics devices; (160.6840) Thermo-optical materials; (230.4555) Coupled resonators.

References and links

1. L. Pavesi and G. Guillot, *Optical Interconnects - The Silicon Approach* (Springer-Verlag, 2006).
2. V. R. Almeida, R. R. Panepucci, and M. Lipson, "Nanotaper for compact mode conversion," Opt. Lett. **28**(15), 1302–1304 (2003).
3. D. K. Sparacin, S. J. Spector, and L. C. Kimerling, "Silicon waveguide sidewall smoothing by wet chemical oxidation," J. Lightwave Technol. **23**(8), 2455–2461 (2005).
4. Q. Xu, B. Schmidt, S. Pradhan, and M. Lipson, "Micrometre-scale silicon electro-optic modulator," Nature **435**(7040), 325–327 (2005).
5. D. J. Thomson, F. Y. Gardes, Y. Hu, G. Mashanovich, M. Fournier, P. Grosse, J.-M. Fedeli, and G. T. Reed, "High contrast 40Gbit/s optical modulation in silicon," Opt. Express **19**(12), 11507–11516 (2011).
6. V. R. Almeida, C. A. Barrios, R. R. Panepucci, and M. Lipson, "All-optical control of light on a silicon chip," Nature **431**(7012), 1081–1084 (2004).
7. P. Dong, W. Qian, H. Liang, R. Shafiiha, D. Feng, G. Li, J. E. Cunningham, A. V. Krishnamoorthy, and M. Asghari, "Thermally tunable silicon racetrack resonators with ultralow tuning power," Opt. Express **18**(19), 20298–20304 (2010).
8. P. Prabhathan, Z. Jing, V. M. Murukeshan, Z. Huijuan, and C. Shiyi, "Discrete and fine wavelength Tunable Thermo-Optic WSS for Low Power Consumption C + L Band Tunability," IEEE Photon. Technol. Lett. **24**(2), 152–154 (2012).
9. W. S. Fegadolli, V. R. Almeida, and J. E. B. Oliveira, "Reconfigurable silicon thermo-optical device based on spectral tuning of ring resonators," Opt. Express **19**(13), 12727–12739 (2011).
10. R. Boeck, N. A. Jaeger, N. Rouger, and L. Chrostowski, "Series-coupled silicon racetrack resonators and the Vernier effect: theory and measurement," Opt. Express **18**(24), 25151–25157 (2010).
11. T. Claes, W. Bogaerts, and P. Bienstman, "Experimental characterization of a silicon photonic biosensor consisting of two cascaded ring resonators based on the Vernier-effect and introduction of a curve fitting method for an improved detection limit," Opt. Express **18**(22), 22747–22761 (2010).
12. T. Claes, W. Bogaerts, and P. Bienstman, "Vernier-cascade label-free biosensor with integrated arrayed waveguide grating for wavelength interrogation with low-cost broadband source," Opt. Lett. **36**(17), 3320–3322 (2011).
13. H. L. R. Lira, S. Manipatruni, and M. Lipson, "Broadband hitless silicon electro-optic switch for on-chip optical networks," Opt. Express **17**(25), 22271–22280 (2009).
14. E. J. Klein, "Densely integrated microringresonator based components for fiber-to-the-home applications," Ph.D. thesis, University of Twente (2007). doc.utwente.nl/60711/1/thesis_E_J_Klein.pdf.
15. H. L. R. Lira, C. B. Poitras, and M. Lipson, "CMOS compatible reconfigurable filter for high bandwidth non-blocking operation," Opt. Express **19**(21), 20115–20121 (2011).
16. W. S. Fegadolli, J. E. B. Oliveira, and V. R. Almeida, "Highly linear electro-optic modulator based on ring

#165009 - $15.00 USD Received 23 Mar 2012; revised 23 May 2012; accepted 28 May 2012; published 15 Jun 2012

resonator," Microw. Opt. Technol. Lett. **53**(10), 2375–2378 (2011).
17. O. Schwelb, "The nature of spurious mode suppression in extended FSR microring multiplexers," Opt. Commun. **271**(2), 424–429 (2007).
18. S. Darmawan and M. K. Chin, "Critical coupling, oscillation, reflection, and transmission in optical waveguide-ring resonator system," J. Opt. Soc. Am. B **23**(5), 834–841 (2006).
19. T. Bååk, "Silicon oxynitride; a material for GRIN optics," Appl. Opt. **21**(6), 1069–1072 (1982).
20. A. H. Atabaki, E. Shah Hosseini, A. A. Eftekhar, S. Yegnanarayanan, and A. Adibi, "Optimization of metallic microheaters for high-speed reconfigurable silicon photonics," Opt. Express **18**(17), 18312–18323 (2010).

1. Introduction

Silicon photonics has been considered a very promising technology, mainly due to its intrinsic characteristic of allowing high integration of optical devices in small footprints and to its synergy with existing CMOS processes, promising to be useful in a wide range of applications, comprising: conventional long-distance down to intra-chip communications, optical sensors in general, as well as many others [1].

Several research groups have developed essential building blocks and proof-of-concept devices overcoming some of the challenges of Silicon platforms, for example: efficient coupling systems from optical fibers to optical waveguides [2], low-loss optical waveguides [3], resonators [4], electro-optic devices [4, 5], all optical devices [6], tunable thermo-optical devices [7, 8], devices insensitive to temperature [9], amongst many others.

However, there are still many challenges that need to be overcome in order to consolidate this technology and allow the integration of large systems, with a myriad of functionalities in a single photonic chip based on Silicon platform.

In this work, we present a reconfigurable thermo-optical switch based on Vernier effect [10–14] control by means of a device structure that contains a pair of coupled ring resonators with micro-heaters on top of them, as schematically depicted in Fig. 1. Such a device is promising to be useful in applications that require optical signal processing, such as equalization, filtering, and switching of optical signals [1].

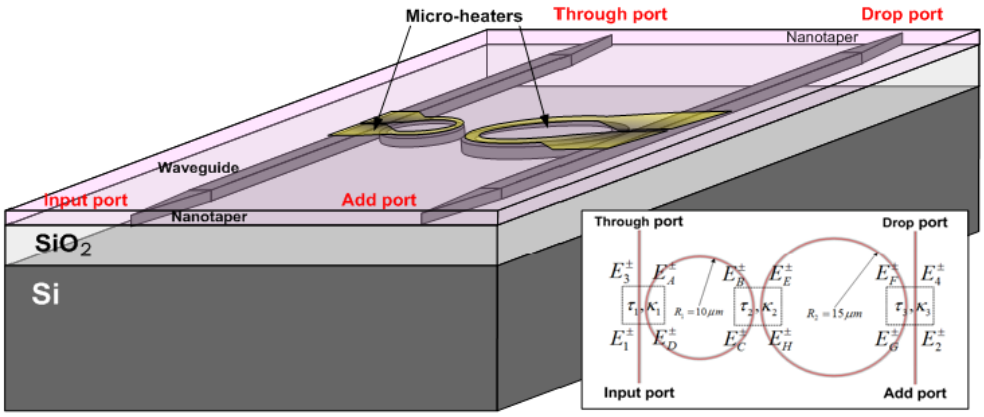

Fig. 1. Schematic representation of the device.

The Vernier effect is an effective and well known approach to increase the free spectral range (FSR) of devices based on resonant cavities, leading to desirable characteristics in applications such as optical sensors and building blocks for communication systems [10–14]. In spite of the existence of several successful demonstrations [14], some researchers consider the mechanism difficult to be harnessed due to the precise optical phase matching between both ring resonators [8, 15].

In order to overcome the foreseen difficulties of phase matching, the principle of operation of our proposed device consists on individually controlling the optical length of each ring resonator. This is achieved by introducing micro-heaters on top the ring resonators, allowing fine adjustments in phase matching between both ring resonators. To our knowledge, this is

#165009 - $15.00 USD Received 23 Mar 2012; revised 23 May 2012; accepted 28 May 2012; published 15 Jun 2012

the first report in the literature concerning the asymmetrical use of micro-heaters so close to each other, in order to try to control the optical phase difference between ring resonators.

This paper is organized as follow: in the second section, the proposed device is mathematically analyzed by means of scattering parameters; in the third section, the fabricated device and fabrication process are discussed; in the fourth section, results are presented; and finally, some conclusions are shown.

2. Theoretical approach

Our modeling was based on a hybrid approach composed of 3D-FDTD simulations, which were implemented on a commercial simulation tool from R-Soft Design Group, Inc. and scattering matrix method, similar to the approach adopted in our previous works [9,16].

The general scattering matrix which describes the optical behavior of the device is given by Eq. (1), which in turn, obeys the schematic representation depicted in Fig. 1.

$$\begin{bmatrix} E_1^- \\ E_2^- \\ E_3^- \\ E_4^- \\ E_A^- \\ E_B^- \\ E_C^- \\ E_D^- \\ E_E^- \\ E_F^- \\ E_G^- \\ E_H^- \end{bmatrix} = \begin{bmatrix} 0 & 0 & \tau_1 & 0 & -j\kappa_1 & 0 & 0 & 0 & 0 & 0 & 0 & 0 \\ 0 & 0 & 0 & \tau_3 & 0 & 0 & 0 & 0 & 0 & -j\kappa_3 & 0 & 0 \\ \tau_1 & 0 & 0 & 0 & 0 & 0 & 0 & -j\kappa_1 & 0 & 0 & 0 & 0 \\ 0 & \tau_3 & 0 & 0 & 0 & 0 & 0 & 0 & 0 & 0 & -j\kappa_3 & 0 \\ -j\kappa_1 & 0 & 0 & 0 & 0 & 0 & 0 & \tau_1 & 0 & 0 & 0 & 0 \\ 0 & 0 & 0 & 0 & 0 & 0 & \tau_2 & 0 & 0 & 0 & 0 & -j\kappa_2 \\ 0 & 0 & 0 & 0 & 0 & \tau_2 & 0 & 0 & -j\kappa_2 & 0 & 0 & 0 \\ 0 & 0 & -j\kappa_1 & 0 & \tau_1 & 0 & 0 & 0 & 0 & 0 & 0 & 0 \\ 0 & 0 & 0 & 0 & 0 & 0 & -j\kappa_2 & 0 & 0 & 0 & 0 & \tau_2 \\ 0 & -j\kappa_3 & 0 & 0 & 0 & 0 & 0 & 0 & 0 & 0 & \tau_3 & 0 \\ 0 & 0 & 0 & -j\kappa_3 & 0 & 0 & 0 & 0 & 0 & \tau_3 & 0 & 0 \\ 0 & 0 & 0 & 0 & 0 & -j\kappa_2 & 0 & 0 & \tau_2 & 0 & 0 & 0 \end{bmatrix} \cdot \begin{bmatrix} E_1^+ \\ E_2^+ \\ E_3^+ \\ E_4^+ \\ E_A^+ \\ E_B^+ \\ E_C^+ \\ E_D^+ \\ E_E^+ \\ E_F^+ \\ E_G^+ \\ E_H^+ \end{bmatrix}. \tag{1}$$

In Fig. 1, the symbol E_i^- corresponds to the *i-th* output electric field for the respective output access, as depicted in Fig. 1, E_i^+ corresponds to the *i-th* input electric field counterpart. τ_1 and κ_1 are, respectively, the electric field transmission and coupling coefficient between the ring resonator 1 and the bus waveguide; τ_2 and κ_2 are, respectively, the electric field transmission and coupling coefficient between the ring resonator 1 and ring resonator 2; τ_3 and κ_3 are, respectively, the electric field transmission and the coupling coefficient between the ring resonator 2 and the add-drop bus waveguide.

Applying the initial condition that only port 1 is optically fed; the optical fields in each input access are given by:

$$\begin{bmatrix} E_1^+ \\ E_2^+ \\ E_3^+ \\ E_4^+ \\ E_A^+ \\ E_B^+ \\ E_C^+ \\ E_D^+ \\ E_E^+ \\ E_F^+ \\ E_G^+ \\ E_H^+ \end{bmatrix} = \begin{bmatrix} E_{in} \\ 0 \\ 0 \\ 0 \\ 0 \\ E_A^- e^{-j\phi_1/2} \\ 0 \\ E_C^- e^{-j\phi_1/2} \\ E_F^- e^{-j\phi_2/2} \\ 0 \\ E_H^- e^{-j\phi_2/2} \\ 0 \end{bmatrix}. \tag{2}$$

#165009 - $15.00 USD Received 23 Mar 2012; revised 23 May 2012; accepted 28 May 2012; published 15 Jun 2012

Thus, replacing Eq. (2) in Eq. (1), one can have the general system of equations which describes the electric fields at output ports of the device as a function of the electric field at input port:

$$\begin{bmatrix} E_3^- \\ E_4^- \\ E_A^- \\ E_C^- \\ E_F^- \\ E_H^- \end{bmatrix} = \begin{bmatrix} \tau_1 & 0 & -j\kappa_1 & 0 & 0 & 0 \\ 0 & 0 & 0 & 0 & -j\kappa_3 & \tau_3 \\ -j\kappa_1 & 0 & \tau_1 & 0 & 0 & 0 \\ 0 & \tau_2 & 0 & -j\kappa_2 & 0 & 0 \\ 0 & 0 & 0 & 0 & \tau_3 & -j\kappa_3 \\ 0 & -j\kappa_2 & 0 & \tau_2 & 0 & 0 \end{bmatrix} \begin{bmatrix} E_{in} \\ E_A^- e^{-j\phi_1/2} \\ E_C^- e^{-j\phi_1/2} \\ E_F^- e^{-j\phi_2/2} \\ E_H^- e^{-j\phi_2/2} \\ 0 \end{bmatrix}, \quad (3)$$

ϕ_1 and ϕ_2 are the accumulated optical phases due to the propagation inside ring resonators 1 and 2, respectively, given by:

$$\phi_1 = \frac{2\pi}{\lambda_0} n_{eff} \left(2\pi R_1\right), \; \phi_2 = \frac{2\pi}{\lambda_0} n_{eff} \left(2\pi R_2\right), \quad (4)$$

where λ_0 is the free space wavelength, n_{eff} is the temperature sensitive complex effective index of refraction for ring resonators and waveguides, and R_i (i = 1, 2) is the radius of the ring resonator.

The main output electric fields in our analysis are E_3^- and E_4^-; they represent, respectively, the electric field at the *through* and *drop output ports* and the solution of the equations system described in Eq. (3) provides us the theoretical general optical behavior of this device.

It is worth pointing out that other authors have developed a similar model to assess coupled ring resonator structure using similar approaches. In addition, some of those have used it to tailor desired spectrum using the *Vernier effect* and providing a complete analysis regarding coupling/transmission ratio and *Free Spectral Range – FSR* [8, 10–14, 17, 18].

3. Fabrication and characterization

The fabrication process of our device is classified in two different layers: the optical layer and the metal layer. The optical layer was fabricated by means of direct E-beam lithography over silicon on insulator substrate with negative tone E-beam resist, followed by dry etching. A 150 nm low-stress silicon nitride layer was deposited by low-pressure chemical vapor deposition (LPCVD), followed by one micrometer thick layer of silicon dioxide deposited by means of plasma-enhanced chemical vapor deposition (PECVD).

The metal level was built in two steps using aligned photolithography and positive photoresist; the first step consists of photolithography of the micro-heaters followed by 100-nm Nichrome deposition, followed by lift-off; the second step, consisted of contact pad and feedline photolithography, followed by (5 nm/300 nm) Ti/Au deposition and, finally, lift-off. Table 1 shows the design parameters used on the fabrication of the device.

Table 1. Designed parameters for the fabricated device:

Waveguide cross-section	**Width**		**Height**
	450 nm		220nm
Coupling regions	**Gap 1**	**Gap 2**	**Gap 3**
	200 nm	500 nm	200 nm
Radii	R_1		R_2
	10 μm		15 μm
Heaters	**Material**	**Thickness**	**Width**
	Nichrome	100 nm	2.5 μm
Pad contacts	**Material**	**Thickness**	**Width**
	Titanium/Gold	5 nm/300 nm	30 μm

#165009 - $15.00 USD Received 23 Mar 2012; revised 23 May 2012; accepted 28 May 2012; published 15 Jun 2012

The *Gap i (i = 1,2,3)* directly affects the field transmission and coupling coefficient, which in turn are related to each other by means of the principle of conservation of energy by $\kappa^2 + \tau^2 = 1$, when losses are disregarded in the coupling regions.

The fabricated device is shown in Fig. 2, where Fig. 2(a) shows the actual device's image obtained by means of an optical microscope and Fig. 2(b) shows the image taken by means of a *Scanning Electron Microscope - SEM*.

Our heaters were designed with a polygonal shape instead of a perfect circular shape in order to maximize the gap between heaters, allowing photolithography process, and still covering a considerable area on top of the ring resonators. The actual computer-aided-design used is shown in the inset on Fig. 2(b).

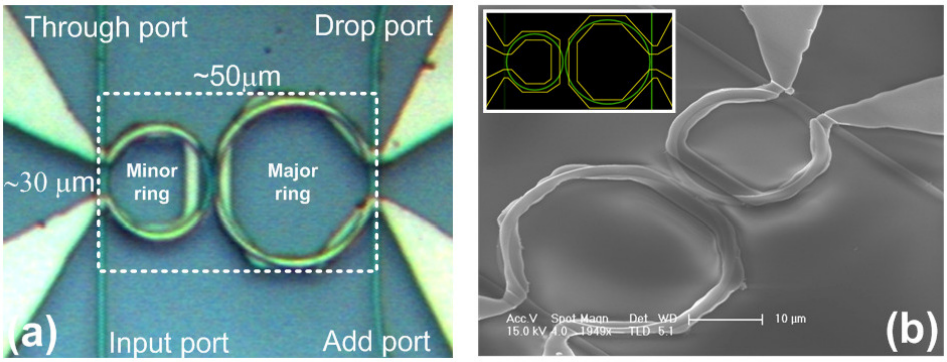

Fig. 2. (a) Device's photograph took from optical microscope; (b) Device's micrograph took from SEM.

One can observe that our heaters show roughness due to an intrinsic limitation of the current fabrication process. An alternative solution to improve roughness using an inversion process is possible.

We analyzed the electrical properties of our heaters by means of a semiconductor analyzer and scanned the electrical current versus voltage in order to measure the resistance of our heaters, which are 650Ω for the major heater and 550Ω for the minor one. In addition, the measured gap between heaters is approximately 2.5µm as per the original design.

Optical measurements used nano-positioners to align polarization maintaining lensed optical fibers into the sample. An agilent tunable laser model 81980A with working band ranging from 1465nm to 1575nm was used as light source and an agilent fiber-coupled power meter model 81636B was used to measure transmitted signals. All optical transmission results in this manuscript were normalized to the maximum optical power obtained at the through port of the device. A temperature controller set to 20°C was used during all measurements in order to reduce thermal drifts, and a Keithley precision current source model 2400 was used to control the electrical current passing through the micro-heaters.

4. Working principle and results

So far, we have discussed just the theoretical approach and fabrication process used in our device; in this section, we discuss its functionalities and its working principle.

Figures 3(a) and 3(c) show, respectively, the theoretical and experimental device's optical response when no bias current is applied on the micro-heaters and when 8 mA are applied on micro-heater over the major ring resonator, which is defined as the ring with larger radius and pointed out in Fig. 2(a). One can observe in Fig. 3(a) the Vernier resonance at 1547.6nm without any bias on heaters for the Quasi-TM polarization, which is fortuitous, but explained by the fact that the resonances for that polarization are broader and easier to obtain the phase matching between them and then demonstrating the Vernier effect. However, in general it is difficult to achieve the precision required during the fabrication process to attain the Vernier resonance for Quasi-TE modes, since small deviation during the fabrication, either during E-

#165009 - $15.00 USD Received 23 Mar 2012; revised 23 May 2012; accepted 28 May 2012; published 15 Jun 2012

beam lithography or the etching process, are enough to introduce phase mismatching between the optical modes; this is one of the reasons why the Vernier Effect is considered, for some researchers, not easy to be experimentally demonstrated [15].

Figures 3(b) and 3(d) show, individually and respectively, the theoretical behavior of each ring resonance when no bias current is applied and when 8 mA is applied on the major ring heater. A similar mathematical approach for each ring resonator was demonstrated in our previous works [9,16].

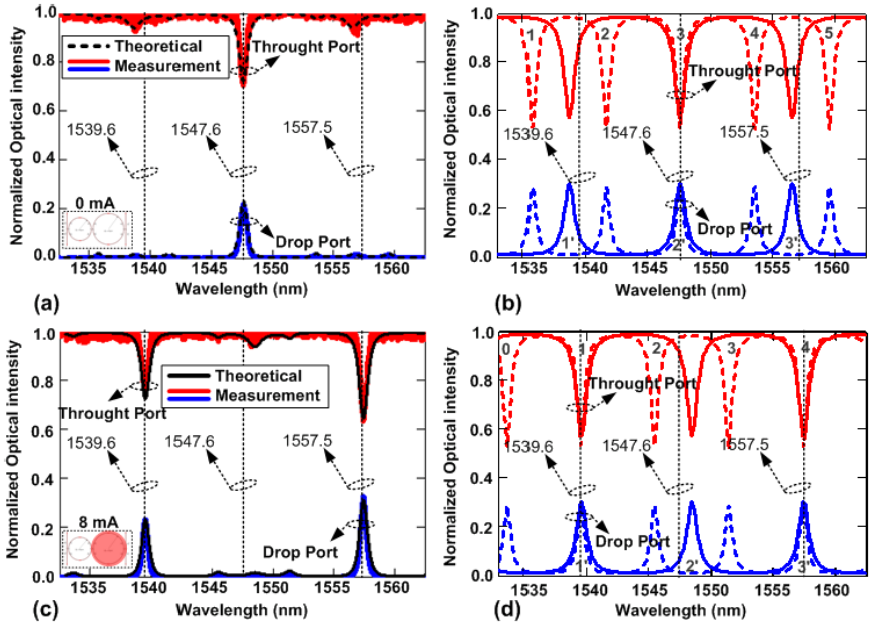

Fig. 3. (a) Theoretical and measured drop/through port optical response when no current is applied on the micro-heaters; (b) individual theoretical optical response of each ring resonator for the behavior observed in (a). (c) Theoretical and measured drop/ through port optical response for 8mA applied on the micro-heater on the major ring resonator. (d) Individual theoretical optical response of each ring resonator under the condition observed in (c). In (b) and (d), the dashed (solid) lines correspond to the optical response for the major (minor) ring resonators, respectively.

Analyzing our device from the *Vernier point of view*, one can observe from Fig. 3(b) that the major ring resonator has five resonances in the spectral window which range from *1530* to *1565 nm*, which are numbered from *1* to *5* on top of the Fig. 3(b); on the other hand, one can observe that the minor ring resonator has only three resonances for the same spectral window, which are numbered from *1'* to *3'* on bottom of Fig. 3(b). The condition showed in Fig. 3(a) and 3(b) shows the original condition in which our device was fabricated without any electrical current applied on micro-heaters, where one can observe that the device was fabricated to have a common resonance at the wavelength of *1547.6 nm*, which means that resonances number *3* and *2'* are in phase to each other, establishing a resulting resonance in this wavelength as demonstrated in Fig. 3(a) by means of theoretical and experimental results, while the others individual resonances, which are not in phase to each other, are suppressed.

Figures 3(c) and 3(d) show the device's optical response of each ring resonator when heating is applied on the major heater. In addition, physically this heat increases the temperature of the minor ring as well, and one can observe that both, the major and minor rings' resonances are affected; however, the minor ring resonator is less affected. A new matching condition is found when the major heater is heated up with electrical current of 8 mA, and then resonances 3 and 2' leave the phase matching condition and *1* and *1',* and *4* and

#165009 - $15.00 USD Received 23 Mar 2012; revised 23 May 2012; accepted 28 May 2012; published 15 Jun 2012

3′ establish phase matching condition at a wavelength of 1539.6 nm and 1557.5 nm, as showed in Fig. 3(d).

In our model, all dispersive functions, such as field transmission coefficients, effective index of refraction for ring waveguides, and loss were fitted to the experimental results. Figure 3 shows the calculated transmission with the extracted parameters as well as the experimental results. Figure 4 summarizes the extracted parameters from the fitting process. Figures 4(a) and 4(b) show, respectively, electric field transmission as a function of wavelength used in our theoretical model for gaps of, respectively, 200nm and 500nm. Figures 4(c) and 4(d) show, respectively, the effective index of refraction and the power loss coefficient for ring waveguides as a function of wavelength.

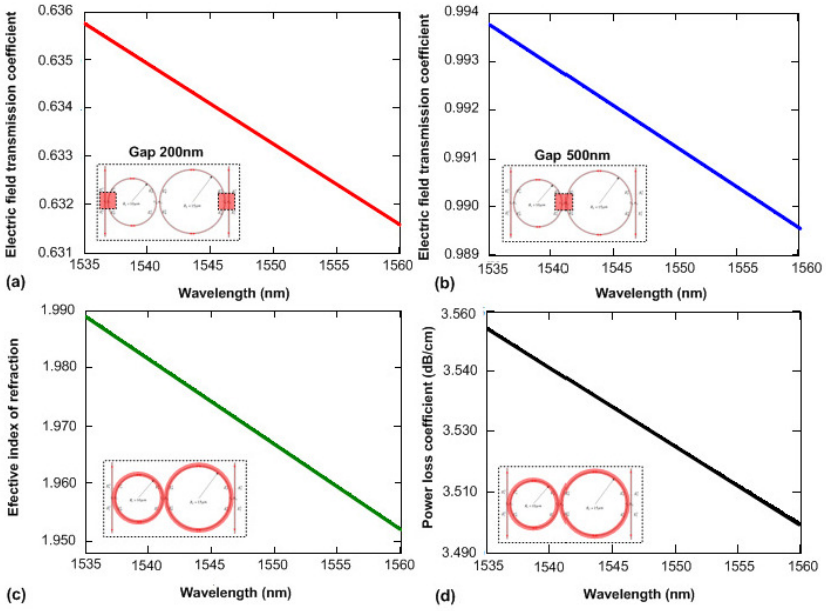

Fig. 4. (a) and (b) show the extracted behavior of the electric field transmission coefficient as a function of wavelength for gaps of, respectively, 200nm and 500nm; (c) extracted behavior of the effective index of refraction for bent ring waveguides as a function of wavelength, and (d) extracted behavior of the power loss coefficient as a function of wavelength for the bent ring waveguides.

Our semi-analytical model allows us to insert an index of refraction variation with temperature. Figure 5(a) shows the simulated theoretical effective index of refraction for a straight waveguide as a function of wavelength and temperature. Figure 5(b) shows the temperature sensitivity for three distinct wavelengths of interest. The results shown in Fig. 5 were obtained with a 3D-mode solver from Rsoft Design Group, Inc., Sellmeier dispersions for Silicon and Silicon dioxide were considered, as well as the dispersion for Silicon nitrate [19].

#165009 - $15.00 USD Received 23 Mar 2012; revised 23 May 2012; accepted 28 May 2012; published 15 Jun 2012

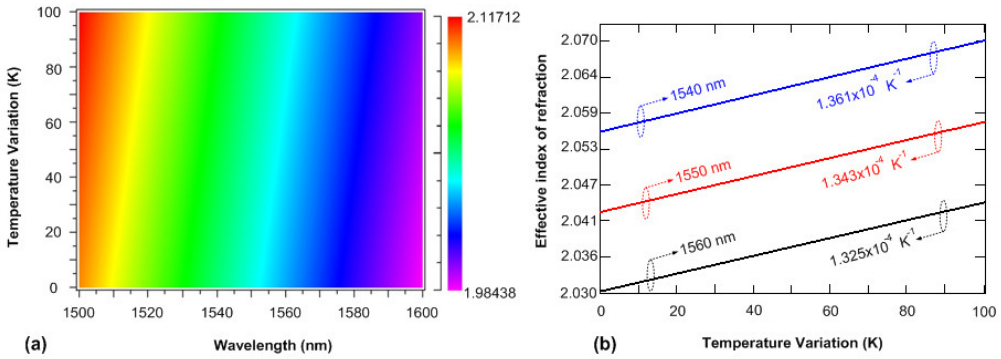

Fig. 5. (a) Theoretical effective index of refraction for a straight waveguide as a function of temperature and wavelength; (b) waveguide sensitivity for three distinct wavelength of interest.

Comparing Figs. 5 and 4(c), one can notice that there is a small discrepancy between the values for the effective index of refraction; this is because Fig. 5 shows a straight waveguide simulation, and Fig. 4(c) is the extracted behavior of the effective index of refraction for a bent waveguide. We considered a straight waveguide to assess the temperature sensitivity of our waveguide owing to the intrinsic limitations of our design tool to perform simulations of bent waveguides with small bending radius.

Based on numerical results shown in Fig. 5, one can observe that the temperature sensitivity of straight waveguide is only slightly wavelength dependent; therefore, in order to simplify our analysis, we assumed that it was constant and took the value for 1550 nm, since our spectral analysis window provide a numerical maximum error of approximately 2%. These sensitivity values were used on the theoretical curve presented in Fig. 3(c) allowing us to predict the average influence of the heating profile in each ring resonator and the rate with which each one is affected by the heating profile.

Our semi-analytical model allows us to assess the behavior of the device based on the effective index of refraction variation; thereby, to assess the influence of the thermal mode in each ring resonator, we developed a systematic algorithm to fit our semi-analytical model with experimental results.

We performed optical transmission measurements in two situations when applying electrical current in the micro-heaters. First, driving only the major heater; secondly, driving simultaneously both heaters. The resonant peak shift was used by our algorithm to extract the average effective index of refraction variation for each ring in both cases. The results are shown in Fig. 6(a). Figure 6(b) shows the extracted effective index of refraction variation as function of temperature, allowing the prediction of the average temperature in each ring resonator.

#165009 - $15.00 USD Received 23 Mar 2012; revised 23 May 2012; accepted 28 May 2012; published 15 Jun 2012

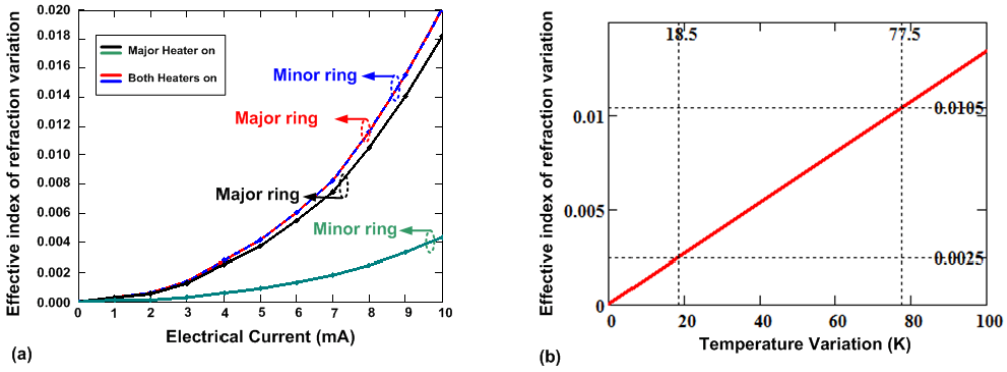

Fig. 6. (a) Extracted behavior of the effective index of refraction as a function of electrical current based on fitting on experimental measurements (Media 1 and Media 2); (b) effective index of refraction variation as a function of temperature variation for 1550nm.

Figure 6(a) shows us that the average change on the effective index of refraction as a function of the electric current obeys a ratio of 4.2:1 when just the major micro-heater current is set turned on, *i.e.*, under this condition the major ring is 4.2 times more sensitive to heating by its heater, than the minor ring. This is an indirect measure of the thermal crosstalk of the device.

On the other hand, when both micro-heaters are turned on with the same electrical current amplitude passing through them, it was observed that the shape of resonance is kept and the peak just shifts, providing the second condition observed in Fig. 6(a). It shows evidences that the average temperature is almost the same in the ring resonators when both heaters are set turned on. In addition, under that working condition, one can observe that both rings set turned on provide more heating to the major ring resonator, another effect of the thermal crosstalk behavior.

The effect of the heating provides phase difference information on each ring resonator; therefore, based on Figs. 6(a) and 6(b), one can state that the average index of refraction variation along the ring resonators is approximately equivalent to an average temperature variation of 18.5K (Δn_{eff} = 2.5x10^{-3}) along the minor ring resonator and 77.5K (Δn_{eff} = 10.5x10^{-3}) on major one when 8 mA is applied in the major heater. This gives us a good understanding of the thermal behavior of that structure, based only on our optical theoretical model.

In order to gain general understanding regarding the thermal behavior of our structure, we simulated its thermal behavior by means of simple *2D-Finite Elements* method, similar to the work performed by Atabaki [20]. Normalized thermal mode profiles are shown in Fig. 7.

Figure 7(a) shows temperature distribution in the case of a heater above a straight optical waveguide. Figures 7(b) and 7(c) show the 2-D temperature distribution when electrical current is applied to the major heater, and to both heater, respectively. Figures 7(d) and 7(e) show the thermal mode in the cross section of the coupling region between both ring resonators when electrical current is applied to the major ring heater, and to both heaters, respectively.

The highlighted arrows in Figs. 7(b) and 7(c) indicate the position where the simulations shown in Figs. 7(a), 7(d), and 7(e) were performed. It is worthy pointing out that Figs. 7(a), 7(d), and 7(e) are not cut views from Figs. 7(b) and 7(c); these are distinct 2D simulation considering the heater position atop, that is why there is a visual discrepancy between the thermal overlap among the cross section and the top view Figs., since with simple 2D simulations one cannot take into account the whole behavior of the structure.

#165009 - $15.00 USD Received 23 Mar 2012; revised 23 May 2012; accepted 28 May 2012; published 15 Jun 2012

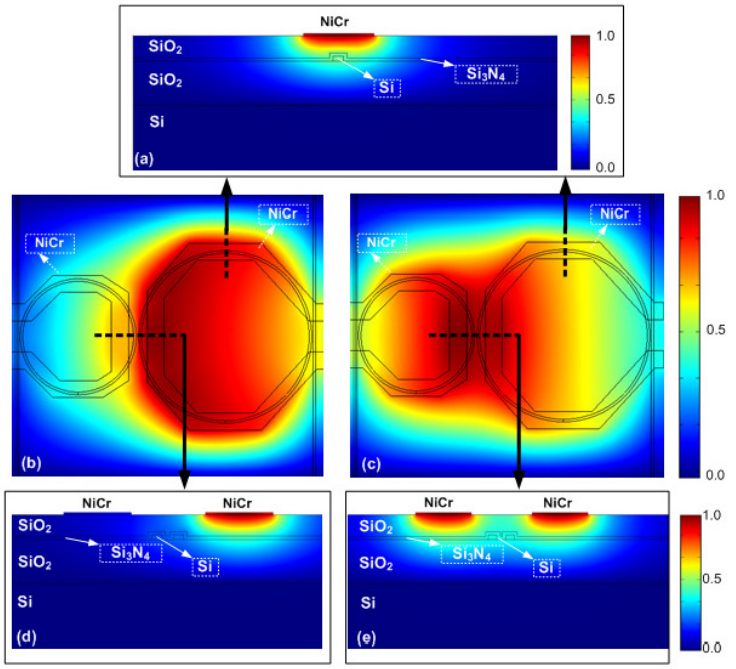

Fig. 7. General theoretical thermal mode behavior provided by NiCr heaters under following conditions: (a) waveguide cross section with micro heater on top, (b) top view when just the major heater is submitted to electrical current, (c) top view when both heaters are submitted to the same electrical current amplitude. (d) waveguide cross section of the coupling region between ring resonators when the major ring is submitted to electrical current and (e) when both are submitted to the same electrical current amplitude.

The asymmetric heating provides an important physical design tool to demonstrate reconfigurability in such devices; as demonstrated in Figs. 3(a) and 3(c), it allows use of this device as a multichannel reconfigurable switch or filter, processing independently wavelengths from only one structure. Figure 8(a) shows the experimental measurements of the optical response at output drop port as a function of the current evolution applied on the major heater. Figure 8(b) shows the extracted behavior of each ring resonator's resonance as a function of electrical current based on the measured optical response and fitting with our semi-analytical model.

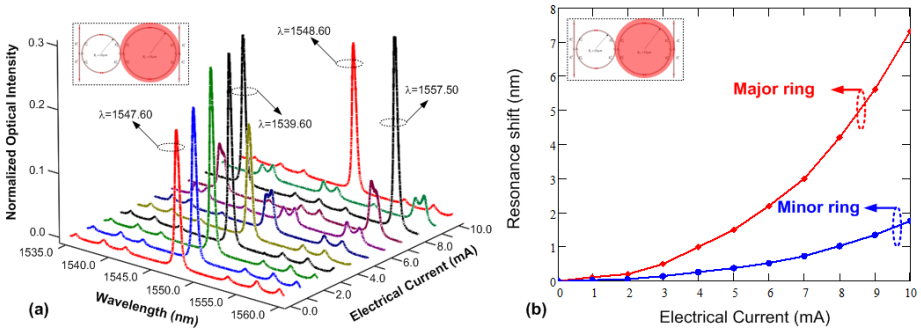

Fig. 8. (a) Measured device's optical response (drop port) as a function of wavelength and electrical current applied on the major micro-heater. See Media 1 to see theoretical behavior for through and drop port as a function of the change of effective index of refraction (Media 1), (b) extracted behavior for each resonance peak shift as a function of electrical current.

#165009 - $15.00 USD Received 23 Mar 2012; revised 23 May 2012; accepted 28 May 2012; published 15 Jun 2012

Amongst the characteristics observed in Fig. 8(a), it is evident that our device is able to optimize the phase matching between resonances, as one can observe from the increased in optical intensity for the currents from 1 mA to 3 mA, establishing a fine tunable adjust of the Vernier effect optical coupled resonance.

Moreover, from 4 to 8 mA, one can observe that the coupled signal quickly reduces. This is due to the transition which establishes the phase mismatching and decoupling at 1547.60 nm, followed by subsequent matching condition and coupling between resonances at the wavelengths 1539.6 nm and 1557.5 nm.

Finally, from 8 to 10 mA, the device goes through another coupling between resonances at 1548.6 nm and starts to regenerate its original shape.

In addition to the experimental results shown in Fig. 8, we also investigated the device's optical response when both heaters are submitted to an electrical current of same amplitude. Figure 9(a) shows the drop port optical response when the same amplitude of electrical current is applied to both micro-heaters and Fig. 9(b) shows the extracted behavior of each ring's resonance shift as a function of electrical current based on the measured optical response and fitting with our semi-analytical model.

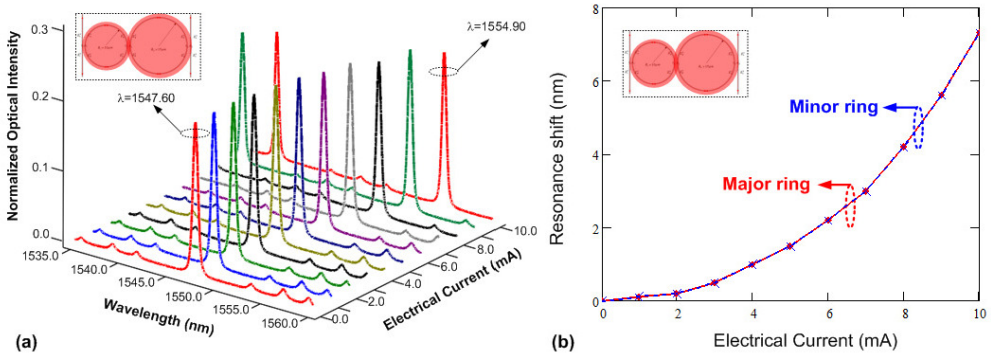

Fig. 9. (a) Measured device's optical response (drop port) as a function of wavelength and electrical current applied on both micro-heaters. See Media 2 to see theoretical behavior for through and drop port as a function of the change of effective index of refraction (Media 2), (b) extracted behavior for each resonance shift as a function of electrical current.

One can observe that the spectral behavior in Fig. 9(a) is quite different from what is shown in Fig. 8(a), in this case the optical response shifts in wavelength. This is due to the fact that the heaters, when submitted to the same electrical current, provide the same power density and hence the temperature in both ring resonators is very close. This in turn does not induce mismatch between the accumulated phase in both ring resonators, keeping the shape of the optical response, but shifting the transmitted peak wavelength.

Based on results presented in Figs. 8 and 7, one can observe that depending on how electrical current is fed into the heaters, the device may enable different shapes or just shift its wavelength, implementing different functionalities, such as tunable filtering/switching, multi-channel switching, non-blocking operation and reconfigurability to be useful in the optical process of signal in general, since we have precise control of the resonance's position and amplitude. These behaviors are expected to be similar for the quasi-TE case but significantly more sensitive to the temperature or current used in the micro-heaters. It is worth pointing out that the insight in the temperature distribution gained from characterizing the quasi-TM mode is very valuable for other polarization conditions.

In this device the maximum extinction ratios for quasi-TM_{00} mode was approximately 3 dB, on the resonant peaks; this is mainly due to the weak coupling condition, between both ring resonators, chosen in our design, which yields a high-Q for the resonances. It is worth pointing out that the electric field transmission coefficient is a relevant parameter to control some figures of merit of our device, such as: extinction ratio, the existence or not of the double peak commonly observed by other authors [11,17,18]; and quality factor Q.

#165009 - $15.00 USD Received 23 Mar 2012; revised 23 May 2012; accepted 28 May 2012; published 15 Jun 2012

5. Conclusions

In summary, the experimentally demonstrated proposed device allows for control of the optical length of individual ring resonators in a partially independent approach. We observed a relation of 4.2:1 in the heating, estimated from the agreement between our theoretical extracted behavior model and the experiment. In addition, we have demonstrated that the proposed device allows a degree of reconfigurability, by enabling changes in intensity and shifting of its optical response. As such, it offers a potential solution to be used in reconfigurable solutions, such as equalization filters, switches and filters in general, allowing all these features into a single and compact device.

Moreover, the asymmetric and compact heating properties, demonstrated in this manuscript, may open the doors for a variety of novel devices, where reconfigurability and active compensation of fabrication deviations are relevant parameters.

Acknowledgment

The authors thank CAPES, CNPq, FAPESP, FOTONICOM, CePOF and the National Science Foundation through NSF ERC Center for Integrated Access Networks (Grant EEC-0812072) and Cornell NanoScale Facility, a member of the National Nanotechnology Infrastructure Network, which is supported by the (Grant ECS-0335765), for financial support. The authors also thank the Electronic Warfare Laboratory at ITA, Photonics Division at IEAv, and the Kavli Nanoscience Institute at Caltech, for the technical support.

#165009 - $15.00 USD Received 23 Mar 2012; revised 23 May 2012; accepted 28 May 2012; published 15 Jun 2012